Bend- and splitting loss of dielectric-loaded surface plasmon-polariton waveguides

Tobias Holmgaard[1], Zhuo Chen[1], Sergey I. Bozhevolnyi[1,2], Laurent Markey[3], Alain Dereux[3], Alexey V. Krasavin[4], and Anatoly V. Zayats[4]

[1]*Department of Physics and Nanotechnology, Aalborg University, Skjernvej 4A, DK-9220, Aalborg Øst, Denmark*

[2]*Institute of Sensors, Signals, and Electrotechnics (SENSE), University of Southern Denmark, Niels Bohrs Allé 1, DK- 5230 Odense M, Denmark*

[3]*Institut Carnot de Bourgogne, UMR 5209 CNRS-Université de Bourgogne, 9 Av. A. Savary, BP 47 870, F-21078 DIJON Cedex, France*

[4]*Centre for Nanostructured Media, IRCEP, The Queens University of Belfast, Belfast BT7 1NN, United Kingdom*

holmgaard@nano.aau.dk

Abstract: The design, fabrication, characterization, and modeling of basic building blocks of plasmonic circuitry based on dielectric-loaded surface polariton waveguides, such as bends, splitters, and Mach-Zehnder interferometers are presented. The plasmonic components are realized by depositing subwavelength dielectric ridges on a smooth gold film using mass-production-compatible UV-photolithography. The near-field characterization at telecommunication wavelengths shows the strong mode confinement and low radiation and bend losses. The performance of the devices is found in good agreement with results obtained by full vectorial three-dimensional finite element simulations.

OCIS codes: (240.6680) Surface plasmons; (250.5300) Photonic integrated circuits; (250.5460) Polymer waveguides

References and links

1. H. Raether, *Surface Plasmons on Smooth and Rough Surfaces and on Gratings*, 1st ed. (Springer-Verlag, Berlin, 1988).
2. R. Zia, J. A. Schuller, A. Chandran, and M. L. Brongersma, "Plasmonics: the next chip-scale technology," Mater. Today **9**, 20–27 (2006).
3. E. Ozbay, "Plasmonics: Merging photonics and electronics at nanoscale dimensions," Science **311**, 189–193 (2006).
4. T. W. Ebbesen, C. Genet, and S. I. Bozhevolnyi, "Surface-plasmon circuitry," Phys. Today **61**, 44–50 (2008).
5. W. L. Barnes, A. Dereux, and T. W. Ebbesen, "Surface plasmon subwavelength optics," Nature (London) **424**, 824–830 (2003).
6. S. A. Maier and H. A. Atwater, "Plasmonics: Localization and guiding of electromagnetic energy in metal/dielectric structures," J. Appl. Phys. **98**, 011101 (2005).
7. S. Lal, S. Link, and N. J. Halas, "Nano-optics from sensing to waveguiding," Nat. Photonics **1**, 641–648 (2007).
8. I. V. Novikov and A. A. Maradudin, "Channel polaritons," Phys. Rev. B **66**, 035403 (2002).
9. S. I. Bozhevolnyi, V. S. Volkov, E. Devaux, J.-Y. Laluet, and T. W. Ebbesen, "Channel plasmon subwavelength waveguide components including interferometers and ring resonators," Nature (London) **440**, 508–511 (2006).

#98719 - $15.00 USD Received 11 Jul 2008; revised 15 Aug 2008; accepted 15 Aug 2008; published 19 Aug 2008

10. V. S. Volkov, S. I. Bozhevolnyi, E. Devaux, J.-Y. Laluet, and T. W. Ebbesen, "Wavelength selective nanophotonic components utilizing channel plasmon polaritons," Nano Lett. **7**, 880–884 (2007).
11. C. Reinhardt, S. Passinger, B. N. Chichkov, C. Marquart, I. P. Radko, and S. I. Bozhevolnyi, "Laser-fabricated dielectric optical components for surface plasmon polaritons," Opt. Lett. **31**, 1307–1309 (2006).
12. B. Steinberger, A. Hohenau, H. Ditlbacher, A. L. Stepanov, A. Drezet, F. R. Aussenegg, A. Leitner, and J. R. Krenn, "Dielectric stripes on gold as surface plasmon waveguides," Appl. Phys. Lett. **88**, 094104 (2006).
13. B. Steinberger, A. Hohenau, H. Ditlbacher, F. R. Aussenegg, A. Leitner, and J. R. Krenn, "Dielectric stripes on gold as surface plasmon waveguides: Bends and directional couplers," Appl. Phys. Lett. **91**, 081111 (2007).
14. T. Holmgaard and S. I. Bozhevolnyi, "Theoretical analysis of dielectric-loaded surface plasmon-polariton waveguides," Phys. Rev. B **75**, 245405 (2007).
15. A. V. Krasavin and A. V. Zayats, "Passive photonic elements based on dielectric-loaded surface plasmon polariton waveguides," Appl. Phys. Lett. **90**, 211101 (2007).
16. S. Massenot, J. Grandidier, A. Bouhelier, G. C. des Francs, L. Markey, J.-C. Weeber, A. Dereux, J. Renger, M. U. Gonzàlez, and R. Quidant, "Polymer-metal waveguides characterization by Fourier plane leakage radiation microscopy," Appl. Phys. Lett. **91**, 243102 (2007).
17. A. V. Krasavin and A. V. Zayats, "Three-dimensional numerical modeling of photonic integration with dielectric-loaded SPP waveguides," Phys. Rev. B **78**, 045425 (2008).
18. T. Holmgaard, S. I. Bozhevolnyi, L. Markey, and A. Dereux, "Dielectric-loaded surface plasmon-polariton waveguides at telecommunication wavelengths: Excitation and characterization," Appl. Phys. Lett. **92**, 011124 (2008).
19. A. Kumar and S. Aditya, "Performance of s-bends for integrated-optic waveguides," Microwave Opt. Technol. Lett. **19**, 289–292 (1998).

1. Introduction

Photonic components based on surface plasmon polaritons (SPPs) have attracted great interest in recent years due to the enticing promise of realizing compact optical circuits with high bandwidths. SPPs, being electromagnetic light waves coupled to collective oscillations in the surface plasma of a metal, are bound to, and propagate along, a metal-dielectric interface. SPPs feature a strong confinement in the direction perpendicular to the metal-dielectric interface due to the exponential field decay away from the interface [1]. They open the possibility of combining the asset of electronics, with respect to size, and photonics, with respect to bandwidth [2, 3, 4]. A key design parameter for realization plasmonic, i.e. SPP-based, components is thus to obtain strong lateral confinement (strong confinement is essential for lower bend losses and higher densities of components) while preserving single-mode operation and keeping propagation losses low. By utilizing nanostructured sub-wavelength-sized metal surfaces, confinement of the SPPs below the diffraction limit is possible [5, 6, 7]. One of the most promising approaches for achieving strong lateral confinement of the SPP fields, simultaneously with relatively low propagation loss, is to utilize V-grooves milled in an otherwise smooth metal surface [8, 9, 10]. This method, however, currently requires complex fabrication techniques using ion-beam milling not applicable for large-scale industrial applications. Another approach for achieving lateral confinement is to employ dielectric-loaded SPP waveguides (DLSPPWs), comprised of dielectric ridges deposited on a smooth gold film [11, 12, 13]. By carefully designing the width and height of the ridges, single-mode propagation and very strong lateral confinement can be achieved with this technology [14, 15, 16, 17]. This promising approach is naturally compatible with different dielectrics and can easily be adapted for industrial fabrication using UV lithography [18]. Here we report the design, fabrication, characterization and modeling of DLSPPW based subwavelength components operating at telecommunication wavelengths.

A metal-dielectric interface is known to support the SPP propagation characterized with the propagation constant β determined by the corresponding dielectric constants, ε_m and ε_d, and light wavelength λ : $\beta = (2\pi/\lambda)[\varepsilon_d\varepsilon_m/(\varepsilon_d+\varepsilon_m)]^{0.5}$ [1]. The real part of β can be related to the SPP effective refractive index, i.e., $N_{eff} = (\lambda/2\pi)Re(\beta)$, implying that the presence of a dielectric layer on the top of a metal surface results in a higher SPP index as compared to a

#98719 - $15.00 USD Received 11 Jul 2008; revised 15 Aug 2008; accepted 15 Aug 2008; published 19 Aug 2008

metal-air interface. Dielectric ridges deposited on the metal surface, known as DLSPPWs [14], can thereby guide SPP modes similarly to conventional dielectric waveguides known in fiber and integrated optics. Comprehensive analysis and simulations conducted for telecommunication wavelengths have shown that, for typical dielectrics with the refractive index of ~ 1.5, the optimum ridge parameters are ~ 500 nm of width and ~ 600 nm of height [14]. Numerical simulations [15, 17] and experimental investigations [11, 18] of DLSPPW components confirmed that DLSPPWs with these parameters are suitable for achieving relatively low bend and propagation losses at telecom wavelengths. We have also demonstrated the possibility of large-scale printing of DLSPPWs with UV lithography [18] rather than writing point-by-point with electron-beam [12, 13] or by using two-photon polymerization lithography [11].

In the present work, we introduce and investigate in detail the operation of basic building blocks of integrated optical circuits: S-bends (i.e., curved bends connecting two parallel waveguides offset with respect to each other), Y-splitters which are composed of two mirrored S-bends and Mach-Zehnder interferometers realized by combining two parallel waveguide sections with two mirrored Y-splitters. All waveguide structures were fabricated using deep UV lithography (wavelength of ~ 250 nm) with a mask aligner in the vacuum contact mode and a ~ 550-nm-thick layer of poly-methyl-methacrylate (PMMA) resist spin-coated on a 60-nm-thin gold film, which was supported by a thin glass substrate. Typically, the width of the produced waveguides, inspected with scanning electron microscopy (SEM), was close to 500 nm ensuring the single-mode (and close to optimum) DLSPPW operation [14]. The performance of the fabricated components was characterized using a collection scanning near-field optical microscope (SNOM) having an uncoated fiber tip used as a probe, and an arrangement for SPP excitation (at $\lambda = 1,500-1,620$ nm) in the Kretschmann-Raether configuration [1], as described in detail elsewhere [18]. All waveguide structures were connected to funnel structures [Fig. 1(a)] facilitating efficient excitation of the DLSPPW mode [18]. However, in contrast with the previous experiments [11, 18], the DLSPPW mode was excited directly inside the taper [Fig. 1(b) and (c)] by matching the excitation angle (in total internal reflection configuration). This resulted in that the recorded SNOM images were of high quality, being practically free from background associated with SPP waves propagating along uncoated areas of the sample (cf. Fig. 1 of this manuscript and Fig. 4 from Ref. [18]).

2. S-bends

The design of S-bends was based on sine curves [19], allowing for continuous bend curvature and thereby adiabatic modification of the DLSPPW mode throughout the bend. Using the SNOM, we characterized several 10-μm-long S-bends with different offsets d, ranging from 2 to 15 μm, and observed for small offsets ($d \leq 5$ μm) excellent performance [Fig. 1(d) and (e)] that gradually deteriorated with the offset increase due to the radiation (into SPP waves) out of the bend [Fig. 1(f) and (g)]. However, even the S-bend with the largest offset ($d = 15$ μm), and the smallest curvature radius of 1.95 μm, transmitted a noticeable amount of DLSPPW mode radiation [Fig. 1(h) and (i)] confirming the strong confinement of the DLSPPW mode.

Bend transmission data (Fig. 2) has been calculated using full vectorial three-dimensional finite element method (3D-FEM) numerical simulations and obtained directly from the SNOM images by averaging the optical signal over a few micro-meters just before and after the S-bend (see Fig. 1(d)). The calculated and measured transmission values were found in good agreement with each other [Fig. 2], and this agreement is also observed in the optical images when comparing the field intensity distributions obtained with the 3D-FEM simulations (see insets in Fig. 2) with the near-field images obtained with the SNOM [Fig. 1]. Note that the transmission shown in Fig. 2 reflects not only the pure bend loss (due to the mode radiation out of the bend) but also the DLSPPW mode propagation loss (due to absorption in gold)

#98719 - $15.00 USD Received 11 Jul 2008; revised 15 Aug 2008; accepted 15 Aug 2008; published 19 Aug 2008

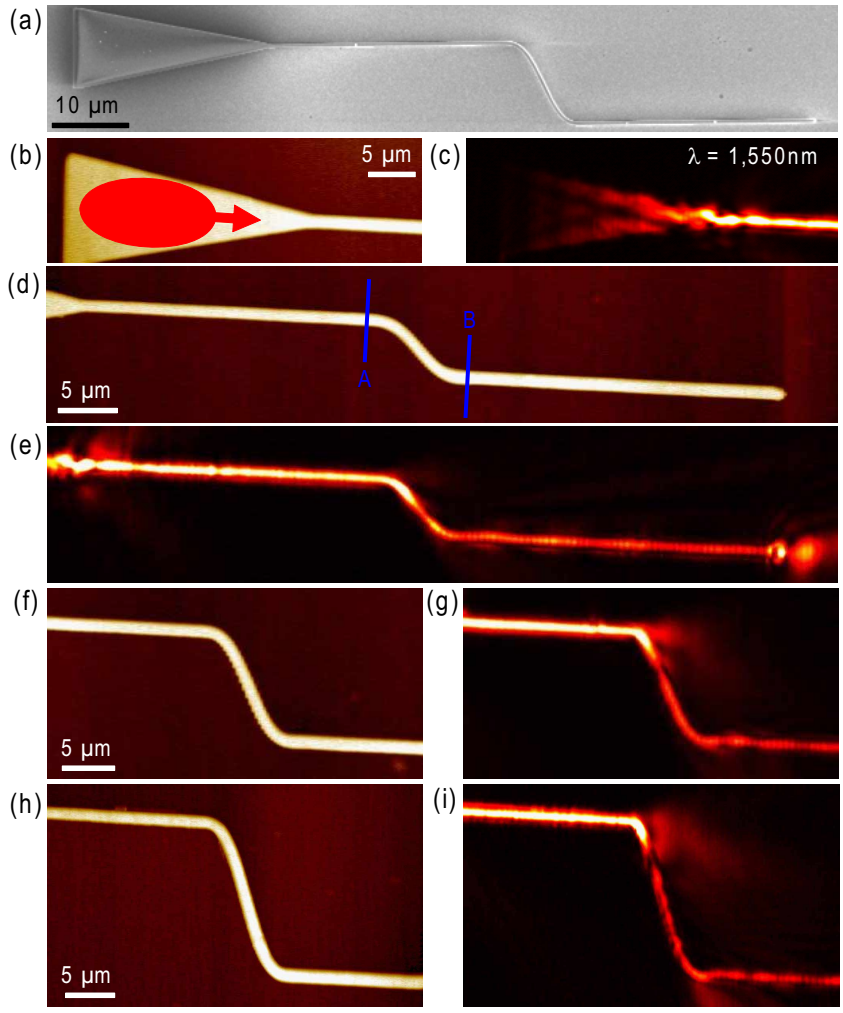

Fig. 1. Plasmonic tapers and S-bends: (a) SEM image of a taper waveguide structure comprising a 10-μm-long S-bend with an offset of 10 μm; (b) topographical and (c) near-field optical ($\lambda = 1,550$ nm) images of the SPP excitation in the taper region and coupling into the single-mode waveguide; (d) topographical and (e) near-field optical ($\lambda = 1,550$ nm) images of the SPP mode propagation in a 10-μm-long S-bend with an offset of 5 μm (note the out-coupling of the SPP waveguide mode into a free-propagating and diverging SPP wave at the waveguide termination). [(f) and (g)] As (d) and (e) but for a waveguide offset of 10 μm. [(h) and (i)] As (f) and (g) but for a waveguide offset of 15 μm.

accumulated over the length of 10-μm-long S-bends. Given the DLSPPW propagation length (whether it being ~ 47 μm as found with the 3D-FEM simulations or ~ 50 μm as obtained from the SNOM images), the pure bend loss is found very small ($< 10\%$) for $d \leq 3$ μm, whereas it constitutes the main loss contribution for $d > 6$ μm.

3. Y-splitters

The performance of 10-μm-long Y-splitters was studied in a similar manner by carrying out the SNOM characterization of Y-splitters fabricated with different arm separations ranging from 3

#98719 - $15.00 USD Received 11 Jul 2008; revised 15 Aug 2008; accepted 15 Aug 2008; published 19 Aug 2008

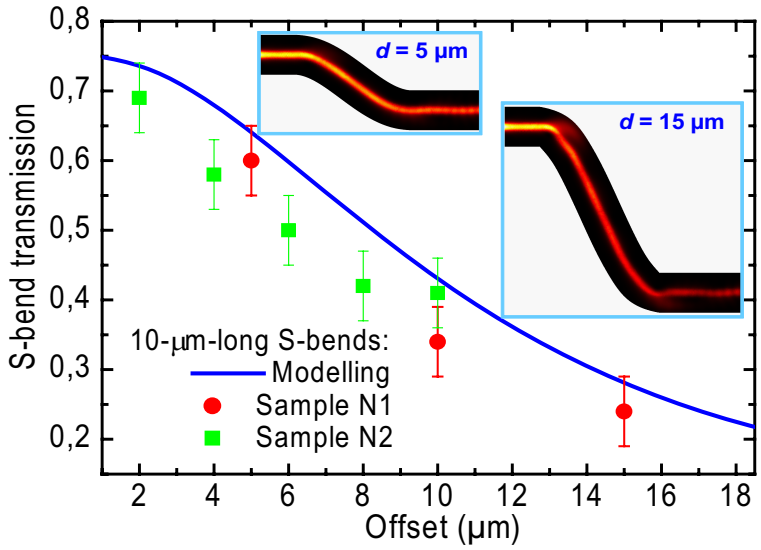

Fig. 2. S-bend transmission dependence on the offset distance between the arms for the 10-μm-long S-bends ($\lambda = 1,550$ nm) determined experimentally from SNOM images (similar to those shown in Fig. 1) and by modeling with 3D-FEM simulations. Insets show calculated intensity distributions in two S-bends with different offsets that should be compared to the optical images shown in Fig. 1(e) and Fig. 1(i). The error bars are obtained from single measurements and, thus, represent the uncertainty in each measurement due to variations in the optical signal.

to 30 μm [Fig. 3]. It is found that the Y-splitters feature pronounced rounding ($\sim$ 300-nm-radius) of the junction area (inset in Fig. 3(b) and (c)) due to limited resolution of the UV-lithography technique used for their fabrication. Such a rounding prevents adiabatic separation of the waveguides and introduces a mismatch between the incoming mode field (into the junction area) and the field of outgoing modes in the waveguide branches, resulting thereby in a transmission loss due to radiation out of the junction as SPP waves propagating in the forward direction on the smooth surface [Fig. 3(c), (e), and (g)]. The occurrence of this radiation along with its influence on the Y-splitter transmission was further verified with the 3D-FEM simulations [Fig. 4]. Simulation of Y-splitters with a 300-nm-radius rounding of the junction area (derived from the SEM image shown as inset in Fig. 3(b) and (c)) shows a $\sim$ 20% decrease in transmission related to the adiabatic splitters, which is in good agreement with the experimentally obtained values. Note that the transmission of adiabatic Y-splitters is expected to be very close to that of the corresponding S-bends (cf. Fig. 2 and Fig. 4), impelling one to improve on the resolution in DLSPPW fabrication, e.g. by exploiting optical proximity correction techniques.

4. Mach-Zehnder interferometers

Upon having achieved efficient splitting of DLSPPW modes, a natural step is to realize a Mach-Zehnder interferometer composed of a Y-splitter followed by two parallel waveguides sections, which are recombined by a mirrored Y-splitter. A 45-μm-long Mach-Zehnder interferometer with an arm separation of 3 μm, consisting of two 10-μm-long Y-splitters and a 25 μm straight waveguide section, has been fabricated and characterized [Fig. 5]. The path lengths of the two waveguide arms are identical as the fabricated Mach-Zehnder interferometer is symmetrical,

#98719 - $15.00 USD Received 11 Jul 2008; revised 15 Aug 2008; accepted 15 Aug 2008; published 19 Aug 2008

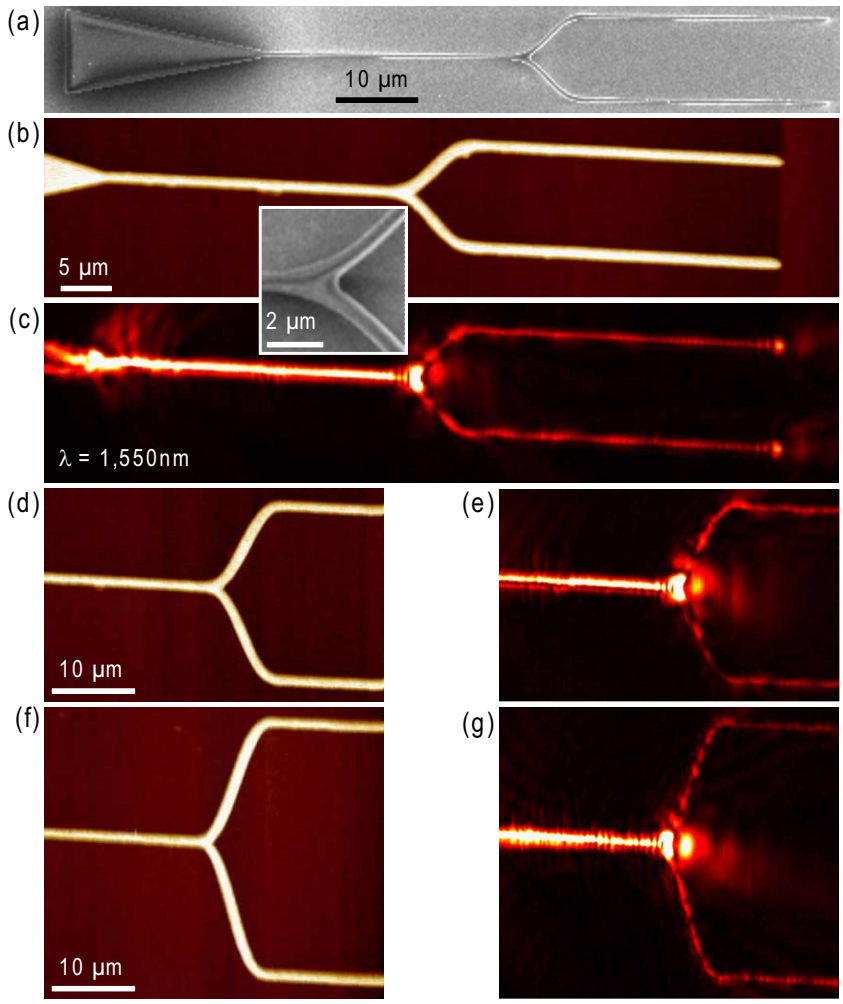

Fig. 3. Plasmonic Y-splitters composed of two mirrored S-bends: (a) SEM image of a taper waveguide structure comprising a 10-μm-long Y-splitter with the arm separation of 10 μm; (b) topographical and (c) near-field optical ($\lambda = 1,550$ nm) images of the Y-splitter shown in (a) along with an inset showing an SEM image of the junction area. [(d) and (e)] As (b) and (c) but for the arm separation of 20 μm. [(f) and (g)] As (d) and (e) but for the arm separation of 30 μm.

and thus constructive interference is expected and indeed observed [Fig. 5(b)], upon recombination of the SPP modes in the two waveguide arms. With an arm length of $\ell \sim 45$ μm and $\lambda = 1,550$ nm, the change in effective index of one arm needed for a switch to complete extinction is $\Delta N_{eff} = \lambda/(2\ell) \sim 1.72 \times 10^{-2}$, which is achievable, e.g., by utilizing thermo-optic effects. The transmission through the 45-μm-long Mach-Zehnder interferometer has been evaluated to ~ 20 %. Due to the overall length of the Mach-Zehnder interferometer the losses are largely dominated by the DLSPPW mode propagation loss accounting for ~ 74 % of the total loss. The fabricated Mach-Zehnder interferometer demonstrates efficient splitting and recombination of the DLSPPW modes as expected from the consideration of Y-splitters above. Furthermore, the near-field optical image confirms the strong lateral confinement of the DLSPPW

#98719 - $15.00 USD Received 11 Jul 2008; revised 15 Aug 2008; accepted 15 Aug 2008; published 19 Aug 2008

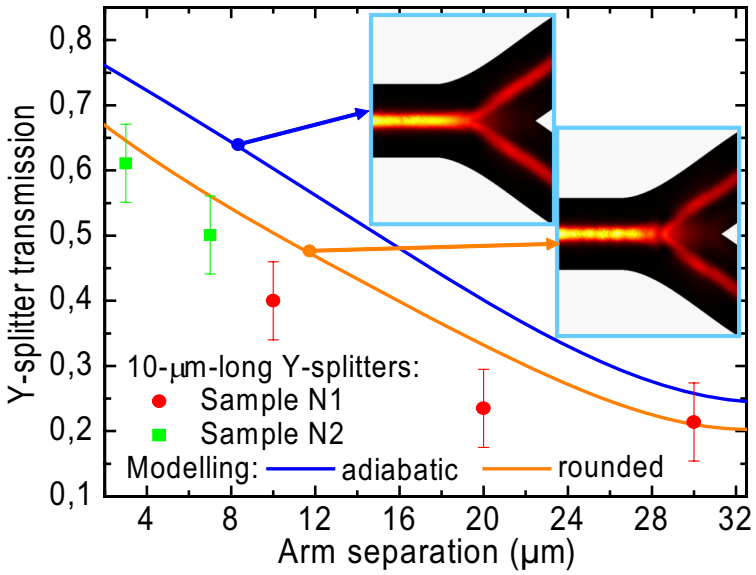

Fig. 4. Transmission of 10-μm-long Y-splitters ($\lambda = 1,550$ nm) as a function of arm separation determined experimentally from the SNOM images similar to the ones shown in Fig. 3 and by modeling with 3D-FEM simulations. Insets show the calculated intensity distributions in 10-μm-wide Y-splitters having adiabatic arm separation and 300-nm-radius rounding of the junction area respectively (the latter should be compared to the optical image in Fig. 3(c)).

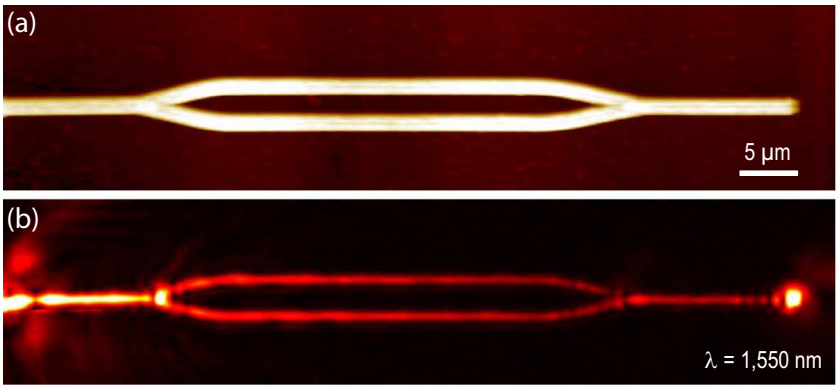

Fig. 5. Mach-Zehnder interferometer with an arm separation of 3 μm: (a) topographical and (b) near-field optical ($\lambda = 1,550$ nm) images, respectively. The SPP mode propagates from left to right.

mode as no mode beating between the parallel waveguides sections is observed [Fig. 5(b)], since the cross-talk is small for 3 μm separation between the waveguides [15, 17].

5. Conclusion

Using industrially compatible large-scale UV-lithography-based fabrication and exploiting the principles of DLSPPW-based plasmonic technology, we have realized compact and low-loss S-bends, Y-splitters and Mach-Zehnder interferometers. The performance of the fabricated pas-

#98719 - $15.00 USD Received 11 Jul 2008; revised 15 Aug 2008; accepted 15 Aug 2008; published 19 Aug 2008

sive plasmonic components has been investigated by applying a SNOM imaging system operating at telecommunication wavelengths, and an excellent correspondence to simulated results, obtained by using the 3D-FEM, has been found. Overall, the SNOM investigations showed that all fabricated basic DLSPPW components, S-bends and Y-splitters, performed as expected in the whole range of laser tunability, exhibiting single-mode and well-confined guiding with the loss level close to calculated, demonstrating thereby robustness to small variations in structural parameters. The pure bend loss of the fabricated S-bends is found very small for small displacements ($d \leq 5\ \mu$m), but dominates the loss contribution for larger displacements. SNOM imaging of Y-splitters demonstrates the realization of a 50/50 splitting of the DLSPPW mode, however, the fabricated Y-splitters exhibit a rounding of the junction area, with a resulting additional radiation loss as compared to an adiabatical split of the waveguide. Thus, the performance of the considered structures could be further improved by perfecting the fabrication (e.g., by using optical proximity correction techniques). The investigated 45 μm-long Mach-Zehnder interferometer, in addition, demonstrates efficient recombination of two DLSPPW modes, yielding a total transmission of ~ 20 %, which can be improved by reducing the overall length of the interferometer (if allowed by the desired functionality), as ~ 74 % of the loss is caused by Ohmic absorption losses during SPP propagation.

Acknowledgments

This work was supported by the FP6 STREP PLASMOCOM (IST 034754). AZ also acknowledges the financial support from EPSRC (UK).

#98719 - $15.00 USD Received 11 Jul 2008; revised 15 Aug 2008; accepted 15 Aug 2008; published 19 Aug 2008